Added Mass and Damping Forces on Circular Cylinders

R. A. SKOP, S. E. RAMBERG, AND K. M. FERER

Applied Mechanics Branch
Ocean Technology Division

March 19, 1976

NAVAL RESEARCH LABORATORY
Washington, D.C.

REPORT DOCUMENTATION PAGE

READ INSTRUCTIONS BEFORE COMPLETING FORM

1. REPORT NUMBER: NRL Report 7970
2. GOVT ACCESSION NO.:
3. RECIPIENT'S CATALOG NUMBER:

4. TITLE (and Subtitle): ADDED MASS AND DAMPING FORCES ON CIRCULAR CYLINDERS

5. TYPE OF REPORT & PERIOD COVERED: Final report on one phase of a continuing program.

6. PERFORMING ORG. REPORT NUMBER:

7. AUTHOR(s): R.A. Skop, S.E. Ramberg, and K.M. Ferer

8. CONTRACT OR GRANT NUMBER(s):

9. PERFORMING ORGANIZATION NAME AND ADDRESS: Naval Research Laboratory, Washington, D.C. 20375

10. PROGRAM ELEMENT, PROJECT, TASK AREA & WORK UNIT NUMBERS: NRL Problems F02-36 and F02-24/Projects P0-4-0009(PDM-03), RR 023-03-45-5807

11. CONTROLLING OFFICE NAME AND ADDRESS: Civil Engineering Laboratory, Port Hueneme, CA, and Office of Naval Research, Washington, D.C.

12. REPORT DATE: March 19, 1976

13. NUMBER OF PAGES: 21

14. MONITORING AGENCY NAME & ADDRESS(if different from Controlling Office):

15. SECURITY CLASS. (of this report): Unclassified

15a. DECLASSIFICATION/DOWNGRADING SCHEDULE:

16. DISTRIBUTION STATEMENT (of this Report)

Approved for public release; distribution unlimited.

17. DISTRIBUTION STATEMENT (of the abstract entered in Block 20, if different from Report)

18. SUPPLEMENTARY NOTES

19. KEY WORDS (Continue on reverse side if necessary and identify by block number)

Fluid forces
Fluid mechanics
Ocean engineering

20. ABSTRACT (Continue on reverse side if necessary and identify by block number)

Results of experiments to determine the fluid loadings on harmonically oscillating circular cylinders show that the inertial (added mass) component of the loading is in good agreement with the inertial loading predicted by potential flow theory. The results show, however, that the commonly used velocity-squared law for damping is inadequate. In fact, experiments indicate that fluid damping is sensibly viscous (linear) for vibration amplitudes up to 0.8 diameter peak-to-peak and is a combination of viscous and velocity-squared damping at larger amplitudes. This new damping law has important implications for the design of offshore structures.

CONTENTS

ADDED MASS AND DAMPING FORCES ON CIRCULAR CYLINDERS

INTRODUCTION

Dynamic analysis of offshore structures subjected to vortex-induced forces, wave-induced forces, earthquakes, or other disturbances requires a knowledge of the fluid added mass and damping forces on the structure. However, the available literature [1,2] contains scant data on these forces, and recourse is usually made to potential flow theory for calculating the added mass forces. The vibrational drag force, meanwhile, is frequently assumed to obey the established drag coefficient-Reynolds number relationship for steady, uniform flow. As stated in Ref. 3, however, the steady relationship "is often used indiscriminately for other flow conditions. This is partly because nothing better is available."

This paper presents the results of a series of tests on the added mass and damping forces on transversely oscillating circular cylinders. Empirical formulas for determining these forces under rather general oscillation conditions are derived. They show that, at least for damping forces, the classical approach is incorrect.

The first part of this paper reviews the mathematics required for interpreting the force measurements. The second part describes the experimental technique. The third part discusses the data reduction methodology and the development of empirical formulas for added mass and damping forces.

MATHEMATICAL FORMULATION

We wish to consider the fluid force per unit length F_f acting on a circular cylinder of diameter d that is constrained to oscillate as $x = x^* \cos \omega t$. Here, x represents the displacement of the cylinder normal to its axis and t denotes time. The amplitude and circular frequency of the oscillation are given respectively by x^* and ω. For the constrained oscillation case, the fluid force per unit length can, in general, be vectorized as

$$F_f(\ddot{x}, \dot{x}) = -m_f(x^*, \omega)\ddot{x} - c_f(x^*, \omega)\dot{x}, \tag{1}$$

where a dot denotes time differentiation. In Eq. (1), m_f is termed the equivalent fluid added mass, and c_f is termed the equivalent fluid viscous damping.. The problem is to measure these quantities and determine their functional dependence on x^* and ω.

To this end, we adopt and approach taken by previous investigators [1,2] — studying the damped, free oscillations of the cylinder. The free oscillation experiment, however, does not match the constrained oscillation conditions for which $m_f(x^*, \omega)$ and $c_f(x^*, \omega)$ are

Manuscript submitted December 24, 1975.

exactly defined. In consequence, inherent differences exist between the added mass and damping values measured in the free oscillation test and those which would be correctly measured in a constrained oscillation test. Prior researchers in this area have failed to recognize these differences. To an extent, this invalidates the interpretations of their experiments. We shall discuss the inherent differences and methods for minimizing them after considering the free oscillation experiment.

Suppose we have performed a free oscillation test and have recorded the amplitude x_i and time of occurrence t_i of each half-cycle peak displacement. Here, $i = 0, 1, 2, \ldots$ represents the half-cycle number, and we define $t_0 = 0$. The data appear typically as in Fig. 1. Note that in this figure a possible nonlinear behavior of the free oscillation is indicated, since it is not known a priori that m_f and c_f are constants over the motion. Thus, our analysis of the data must not be based on preconceived notions of linearity or of particular nonlinearities.

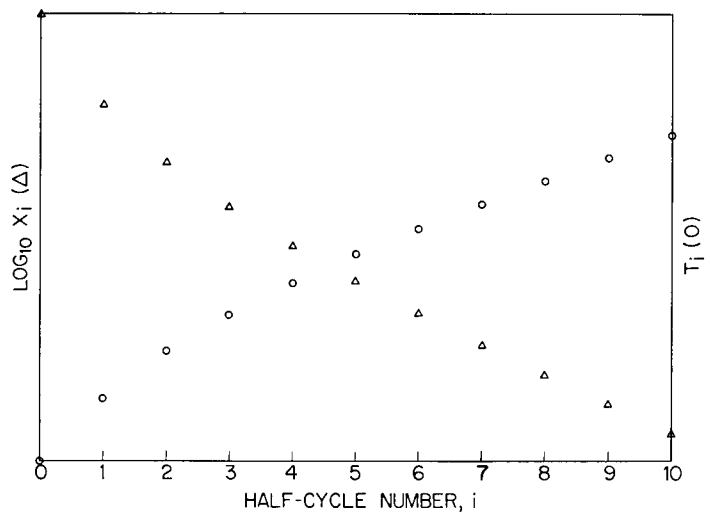

Fig. 1 — Possible form of the data obtained from a free oscillation test

As is known from the theory of nonlinear oscillations (see, for example, Minorsky [4]), the response of a free nonlinear oscillator can be approximated by an equivalent linear oscillator. In particular, the decay law for the free oscillation of the cylinder between the i and $i+j$ half-cycles can be approximated as

$$x_{i+j}/x_i = \exp\left\{-\left[(c + c_f)/2(m + m_f)\right](t_{i+j} - t_i)\right\}. \qquad (2a)$$

Similarly, the frequency $\omega_{i,i+j}$, representing the motion between the i and $i + j$ half-cycles, can be approximated by

$$\omega_{i,i+j} = \pi j/(t_{i+j} - t_i) = [k/(m + m_f)]^{1/2}. \tag{2b}$$

In these equations, m, c, and k denote, respectively, the mass, damping constant, and spring constant, all per unit length of the spring-mounted circular cylinder and, ideally, as measured in a vacuum. Again, m_f and c_f denote the equivalent fluid loadings to be determined.

The above equivalent linear approximation can be shown [4] to have accuracy of order $(dx/x)^2$ to any actual oscillation behavior. Since between the i and $i + j$ half-cycles $dx \approx x_i - x_{i+j}$ and, on the average, $x \approx (x_i + x_{i+j})/2$, we can define an error E_1 associated with the linear approximation to the actual oscillation behavior as

$$E_1 = \left[(x_i - x_{i+j})/(x_i + x_{i+j})\right]^2. \tag{3}$$

This is one inherent error connected with a free oscillation experiment for determining the equivalent fluid loadings. The effect of this error is reflected in the formulas

$$\left[m_f(x^*, \omega) - m_{fm}(\bar{x}, \bar{\omega})\right] / m_{fm}(\bar{x}, \bar{\omega}) \approx E_1 \tag{4a}$$

$$\left[c_f(x^*, \omega) - c_{fm}(\bar{x}, \bar{\omega})\right] / c_{fm}(\bar{x}, \bar{\omega}) \approx E_1, \tag{4b}$$

where the subscript m refers to the measured value.

In writing Eqs. (4), we have also indicated a second inherent error connected with a free oscillation experiment for determining the equivalent fluid loadings; namely, what values of amplitude $\bar{x}$ and frequency $\bar{\omega}$ between the i and $i + j$ half-cycles should be assigned to the measured fluid loadings? We are free to choose these values, but there is no assurance that the numbers we choose are the numbers x^* and ω with which the measured loadings should correctly be associated.

To estimate this second inherent error, we assign the following values to $\bar{x}$ and $\bar{\omega}$ between the i and $i + j$ half-cycles:

$$\bar{x} = (x_i + x_{i+j})/2 \tag{5a}$$

$$\bar{\omega} = \left[\max\ (\omega_{n,n+1}) + \min\ (\omega_{n,n+1})\right]/2, \tag{5b}$$

where $i \leqslant n \leqslant (i + j - 1)$, and $\omega_{n,n+1}$ is defined by Eq. (2b). Equation (5b) says simply that we choose for $\bar{\omega}$ the average of the highest and lowest frequencied half-cycles in the range i to $i + j$. Within this range, we also have limits on x^* and ω given by

$$x_i \geqslant x^* \geqslant x_{i+j} \tag{6a}$$

and

$$\max(\omega_{n,n+1}) \geqslant \omega \geqslant \min(\omega_{n,n+1}). \tag{6b}$$

On calculating the percentage uncertainties between the assigned values and the possible correct values of the amplitude and frequency, we find from Eqs. (5) and (6) that

$$(x^* - \bar{x})/\bar{x} \leqslant E_{\bar{x}} = (x_i - x_{i+j})/(x_i + x_{i+j}) \tag{7a}$$

$$(\omega - \bar{\omega})/\bar{\omega} \leqslant E_{\bar{\omega}} = \left[\max(\omega_{n,n+1}) - \min(\omega_{n,n+1})\right] \Big/ \left[\max(\omega_{n,n+1}) + \min(\omega_{n,n+1})\right]. \tag{7b}$$

Here, $E_{\bar{x}}$ and $E_{\bar{\omega}}$ define the errors associated with our inherent inability to choose the correct values of amplitude x^* and frequency ω that should be assigned to the measured fluid loadings.

Finally, solving Eqs. (2) yields expressions for m_{fm} and c_{fm} in terms of the free oscillation data as

$$m_{fm}(\bar{x}, \bar{\omega}) = k\left[(t_{i+j} - t_i)/\pi j\right]^2 - m \tag{8a}$$

$$c_{fm}(\bar{x}, \bar{\omega}) = \left[2k(t_{i+j} - t_i)/(\pi j)^2\right] \ell n(x_i/x_{i+j}) - c, \tag{8b}$$

with $\bar{x}$ and $\bar{\omega}$ defined by Eqs. (5).

MINIMIZATION OF THE INHERENT ERRORS

The main purpose of the preceding section is to point out the inherent errors of using a free oscillation experiment for determining the equivalent fluid loadings, which are strictly defined only for constrained oscillation conditions. This section discusses the minimization of these errors so that the results are as accurate as available data permit.

The inherent errors are those involved with nonlinearities E_1 and with amplitude and frequency definitions $E_{\bar{x}}$ and $E_{\bar{\omega}}$. These errors are defined by Eqs. (3), (4), and (7). From these equations, it is apparent that each of the errors is minimized by selecting from the data only adjacent (that is, i and i+1) half-cycle peaks. This approach gives $E_{\bar{\omega}} = 0$, so that there is no difference between the assigned and correct vibrational frequencies.

To simplify the notation, we denote by x_0 and x_1, respectively, the amplitudes at the beginning and end of the half-cycle and by τ the duration of the half-cycle. The equivalent fluid loadings obtained from the half-cycle data are then, from Eqs. (8),

$$m_{fm}(\bar{x},\ \omega) = k(\tau/\pi)^2 - m \tag{9a}$$

and

$$c_{fm}(\bar{x},\ \omega) = (2k\ \tau/\pi^2)\ell n(x_0/x_1) - c, \tag{9b}$$

where, from Eqs. (5),

$$\bar{x} = (x_0 + x_1)/2 \tag{10a}$$

$$\omega = \pi/\tau. \tag{10b}$$

The remaining inherent half-cycle errors are defined by Eqs. (7) and (3) as

$$E_{\bar{x}} = (x_0 - x_1)/(x_0 + x_1) \tag{11a}$$

and

$$E_1 = E_{\bar{x}}^2, \tag{11b}$$

and we have, from Eqs. (4) and (7),

$$\left[m_f(x^*,\ \omega) - m_{fm}(\bar{x},\ \omega)\right]/m_{fm}(\bar{x},\ \omega) \approx E_{\bar{x}}^2 \tag{12a}$$

$$\left[c_f(x^*,\ \omega) - c_{fm}(\bar{x},\ \omega)\right]/c_{fm}(\bar{x},\ \omega) \approx E_{\bar{x}}^2 \tag{12b}$$

and

$$(x^* - \bar{x})/\bar{x} \approx E_{\bar{x}}. \tag{12c}$$

DIMENSIONLESS PARAMETERS

Under the constrained oscillation conditions for which the equivalent fluid loadings are strictly defined, the only free variables besides x^*, ω, and the cylinder diameter d are the fluid density ρ and absolute viscosity μ. From the method of indices, we know that these five variables can be reduced to a set of two dimensionless parameters that specify the entire system. We take these two numbers as the dimensionless amplitude α and vibratory Reynolds number β defined by

$$\alpha = x^*/d \tag{13a}$$

$$\beta = \omega d^2/4\nu, \tag{13b}$$

where $\nu = \mu/\rho$ is the kinematic viscosity.

Using the customary definitions for the dimensionless parameters, we can further write

$$m_f(x^*, \omega) = (\pi/4)\rho d^2 C_M(\alpha, \beta) \tag{14a}$$

and

$$c_f(x^*, \omega) = \pi\rho\nu\beta^{1/2} C_V(\alpha, \beta), \tag{14b}$$

where C_M and C_V are the equivalent added mass and viscous damping coefficients. We shall henceforth concern ourselves with the determination of these coefficients. The inherent half-cycle errors defined by Eqs. (12) remain the same for C_M, C_V, and α with obvious notational differences.

EXPERIMENTAL TECHNIQUE

A circular cylindrical rod of known length L, diameter d, and mass per unit length m was supported in a heavy, rigid frame by four identical springs (Fig. 2). Two stops on the frame were positioned by micrometer exactly two diameters above the stationary rod. The rod was pulled up and held against the stops by elastic bands. On signal, the bands were freed simultaeously by two electromechanical releases. Since both the springs and stops were positioned symmetrically with respect to the center of the rod, its motion was purely translatory. This motion was tracked by an electro-optical system (Physitech System Model 441) calibrated to produce an output voltage linearly proportional to the rod displacement over the range ± 2.5 V. The output voltage was plotted vs time on a high-frequency-response stripchart recorder (Sanborn Recording System Model 356).

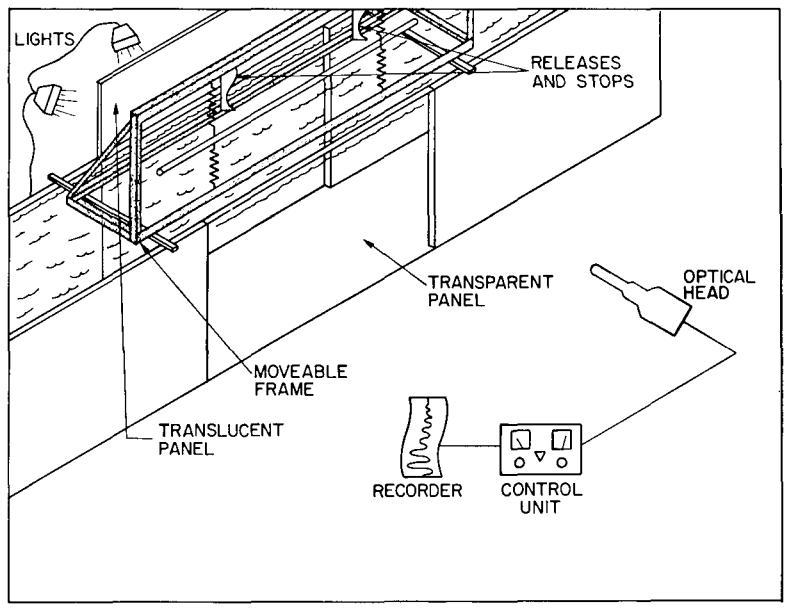

Fig. 2 — The experimental setup

These operations were performed first in air and then in water. The measurements in air were used to calculate the damping constant c and spring constant k from Eqs. (8), under the assumption that in air the fluid loadings were negligible. Care was taken in the selection of springs to ensure that the oscillatory behavior in air was linear over the entire displacement range. A summary of the 30 different combinations of L, d, m, c, and k used in the test series is given in Table 1.

Table 1 — Summary of Experimental Combinations

Data Set	L (cm)	d (cm)	m (g/cm)	c (g/cm s)	k (g/cm s^2)
1	137.01	0.79	3.81	0.126	3,351
2	121.77	0.79	3.79	0.066	920
3	106.81	0.79	3.78	0.079	1,072
4	91.57	0.79	3.78	0.084	1,290
5	76.20	0.79	3.76	0.088	1,501
6	76.20	0.79	3.76	0.219	6,823
7	76.20	0.79	3.76	0.459	14,844
8	76.20	0.79	3.76	0.410	38,191
9	76.20	0.79	3.76	4.753	51,299
10	152.40	1.27	9.93	0.359	4,913
11	137.31	1.27	9.92	0.345	5,361
12	122.07	1.27	9.92	0.259	6,110
13	106.83	1.27	9.95	0.394	6,962
14	91.59	1.27	10.00	0.376	8,317
15	76.35	1.27	9.98	0.552	9,968
16	76.35	1.27	9.98	0.971	15,737
17	76.35	1.27	9.98	1.064	43,025
18	152.55	1.91	21.87	1.758	8,786
19	137.08	1.91	21.89	1.593	9,814
20	124.38	1.91	21.44	1.923	10,727
21	109.14	1.91	21.38	2.162	12,381
22	93.83	1.91	21.31	2.288	14,350
23	78.59	1.91	21.20	2.406	17,251
24	78.59	1.91	21.20	2.816	43,628
25	152.55	2.54	38.87	2.021	23,101
26	137.31	2.54	38.90	2.590	25,314
27	121.92	2.54	38.92	6.041	28,278
28	106.60	2.54	38.93	7.301	32,239
29	91.36	2.54	38.94	7.749	37,667
30	75.97	2.54	38.98	9.490	45,040

During the measurements in water, the minimum distance between the center of the stationary rod and any surrounding surface was at least eight rod diameters. This rendered surface effects negligible. In addition, the ratio of length to diameter of the rod was always greater than 30, to preclude significant end effects. A typical stripchart recording of the oscillatory behavior in water is shown in Fig. 3.

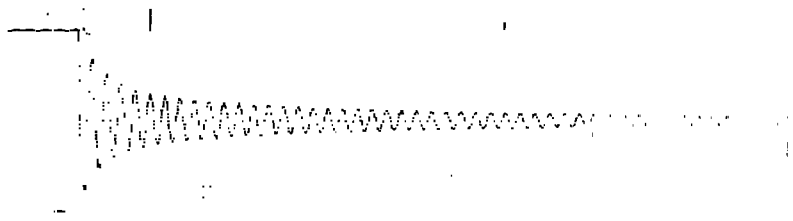

Fig. 3 — Typical stripchart recording of the oscillatory motion in water. The time scale is 25 mm/s, and the amplitude scale is from -2.5 V to +2.5 V. This particular recording corresponds to data set 16.

DATA REDUCTION

For each data set, the half-cycle peak amplitudes x_i and the half-cycle duration τ were measured from the stripchart recording of the oscillatory behavior in water. To within the accuracy of the measurements (errors on the order of 1%), the half-cycle duration was found to be constant for the particular data set. That is, the response frequency in water was found to be independent of the amplitude of oscillation.

The values for the half-cycle peak amplitudes typically appeared as in Figs. 4a and 4b, which show the measurements corresponding to data sets 1 and 16 of Table 1, respectively. To put these decay results in a form useful for further calculations, the data were smoothed by a least-squares curve fitting procedure. The fitting function was chosen as

$$\ell n x_i = B_1 + B_2 e^{-\gamma i} - B_3 i, \tag{15a}$$

and the sum S of the weighted squares of the residuals to be minimized was

$$S = \sum_{i=0}^{N-1} x_i^2 \left[\ell n x_i - \left(B_1 + B_2 e^{-\gamma i} - B_3 i\right)\right]^2, \tag{15b}$$

where N was the number of half-cycle peak amplitudes measured. The weighting function x_i^2 was included since it was the peak amplitudes and not their logarithms that were to be fitted (see Deming [5]). Other functions besides $e^{-\gamma i}$ (in particular, $1/(1 + \gamma i)^q$) were used in attempting to fit the nonlinear decay of $\ell n x_i$ for small i. However, the sums of the weighted, squared residuals obtained with these other functions were at least an order of magnitude larger than the one obtained by using $e^{-\gamma i}$.

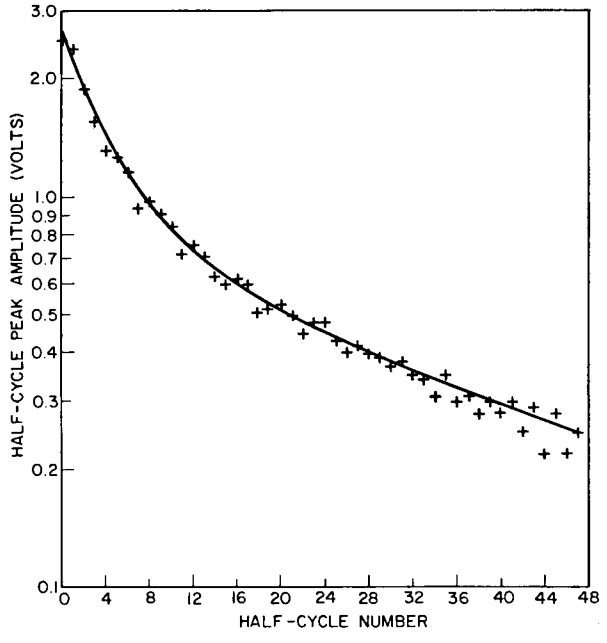

(a)

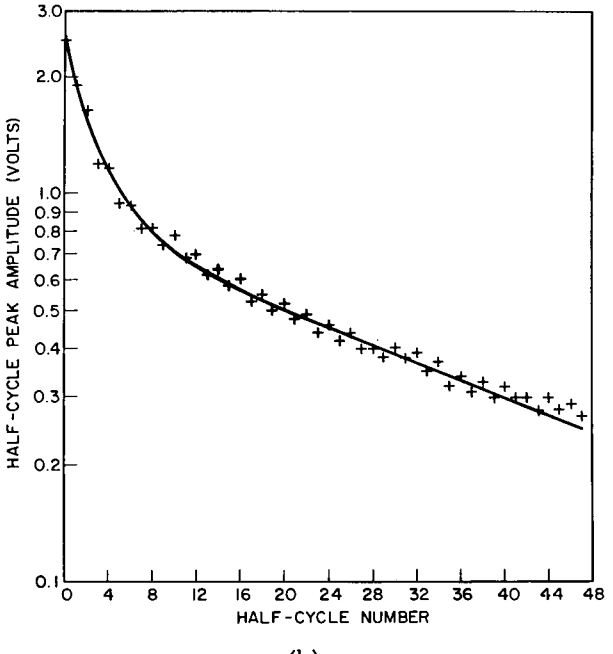

(b)

Fig. 4 — Half-cycle peak amplitudes (in volts) vs half-cycle number (a) for data set 1 and (b) for data set 16. The experimentally measured amplitudes are denoted by the + symbol. The solid line is the least-squares curve fit to the data.

Actually, the smoothing process occurred in two steps, since from the raw amplitude data it was apparent that the stripchart recorder was not exactly zeroed. This is shown clearly in Fig. 4b, where the even half-cycle amplitudes are consistently larger than the preceding odd half-cycle amplitudes, indicating a slightly positive zero offset. To correct for the DC offset, the raw amplitude data were first fit by Eq. (15a). The average offsets A_e and A_o of the even and odd half-cycle amplitudes from the smoothed curve were then calculated as

$$A_e = \frac{1}{N_e} \sum_{i=0}^{N_e-1} \left[x_{2i} - \exp\left(B_1 + B_2 e^{-2\gamma i} - 2B_3 i\right) \right] \tag{16a}$$

and

$$A_o = \frac{1}{N_o} \sum_{i=0}^{N_o-1} \left\{ x_{(2i+1)} - \exp\left[B_1 + B_2 e^{-\gamma(2i+1)} - B_3(2i+1) \right] \right\}, \tag{16b}$$

where N_e and N_o were the number of even and odd half-cycle peaks, respectively. The DC offset was obtained from

$$\mathrm{DC} = (A_e - A_o)/2, \tag{17}$$

and corrected even and odd half-cycle amplitudes x_i' were computed, respectively, as

$$x'_{2i} = x_{2i} - \mathrm{DC}; \quad i = 0, 1, \ldots, N_e - 1 \tag{18a}$$

$$x'_{(2i+1)} = x_{(2i+1)} + \mathrm{DC}; \quad i = 0, 1, \ldots, N_o - 1. \tag{18b}$$

The set of corrected half-cycle peak amplitudes were then refitted by Eq. (15a) to yield final values for B_1, B_2, B_3, and γ. In Figs. (4a) and (4b), the resulting least-squares fit to the amplitude data is shown by the solid line.

A summary of the reduced experimental data is given in Table 2. Listed for each data set, cross-referenced to Table 1, are the number N of half-cycle peak amplitudes measured, the calculated DC offset, the sum S of the weighted, squared residuals corresponding to the final least-square values of B_1, B_2, B_3, and γ, these values, and the frequency f in water.

EMPIRICAL FORMULAS FOR ADDED MASS AND VISCOUS DAMPING

From the information contained in Tables 1 and 2, plus the voltage scaling law, 1 V = $(2d/e^{B_1+B_2})$ diameters, the calculations of the fluid loadings $m_{fm}(\bar{x}, \omega)$ and $c_{fm}(\bar{x}, \omega)$ from Eqs. (9) and, thence, of the added mass and viscous damping coefficients $C_M(\alpha, \beta)$ and $C_V(\alpha, \beta)$ from Eqs. (14) are straightforward. Since the frequency f in water is constant for a particular data set, the vibrational Reynolds number β (Eq. (13b)) associated with the data

Table 2 — Summary of Reduced Data

Data Set	N	DC Offset (V)	S	$\ell nx_i = B_1 + B_2 e^{-\gamma i} - B_3 i$ (Eq. (15a))				f(Hz)
				B_1	B_2	B_3	γ	
1	48	-0.011	0.096	-0.274	1.243	0.0240	0.132	4.40
2	38	-0.002	0.091	-0.233	1.186	0.0384	0.196	2.32
3	45	0.041	0.064	-0.256	1.187	0.0408	0.213	2.50
4	46	-0.004	0.024	-0.238	1.168	0.0396	0.212	2.69
5	46	0.013	0.026	-0.318	1.234	0.0349	0.216	2.97
6	48	0.011	0.039	-0.200	1.111	0.0284	0.205	6.37
7	48	-0.002	0.040	-0.319	1.232	0.0269	0.184	9.40
8	48	0.007	0.026	-0.280	1.182	0.0239	0.183	15.07
9	48	0.014	0.018	-0.109	1.035	0.0333	0.189	17.00
10	48	0.049	0.058	-0.254	1.147	0.0255	0.193	3.33
11	48	-0.020	0.022	-0.217	1.131	0.0235	0.207	3.48
12	48	0.018	0.021	-0.230	1.164	0.0233	0.179	3.75
13	48	0.035	0.054	-0.083	1.026	0.0312	0.207	3.98
14	48	0.017	0.066	-0.434	1.346	0.0262	0.234	4.29
15	48	0.040	0.062	-0.317	1.213	0.0239	0.199	4.75
16	48	0.020	0.029	-0.174	1.084	0.0261	0.251	5.99
17	48	0.016	0.038	-0.195	1.091	0.0298	0.186	9.83
18	48	0.017	0.027	-0.185	1.099	0.0218	0.170	3.01
19	48	0.043	0.032	-0.068	0.973	0.0222	0.179	3.17
20	48	0.008	0.024	-0.151	1.061	0.0210	0.198	3.37
21	48	0.032	0.034	-0.115	1.030	0.0280	0.208	3.60
22	48	0.055	0.072	-0.234	1.142	0.0230	0.211	3.90
23	48	0.046	0.048	-0.177	1.064	0.0222	0.209	4.27
24	48	0.049	0.095	-0.095	0.967	0.0232	0.223	6.83
25	48	0.067	0.118	-0.190	1.059	0.0252	0.266	3.65
26	48	0.026	0.123	-0.079	0.947	0.0248	0.257	3.85
27	48	0.060	0.152	-0.151	1.026	0.0248	0.253	4.07
28	48	0.002	0.150	-0.212	1.104	0.0205	0.238	4.33
29	48	-0.019	0.181	-0.136	1.031	0.0217	0.250	4.69
30	48	0.024	0.202	-0.112	1.000	0.0233	0.226	5.15

set is itself constant. The added mass coefficient $C_M(\alpha, \beta)$ associated with the data set is also constant and independent of the dimensionless vibrational amplitude α (Eq. (13a)). For clarity, we will henceforward abbreviate $C_M(\alpha, \beta)$ by $C_M(\beta)$.

The relationship between the viscous damping coefficient $C_V(\alpha, \beta)$ and the dimensionless amplitude α is typically as in Figs. 5a and 5b, which show the calculated values of $C_V(\alpha, \beta)$ and α corresponding to data sets 1 and 16, respectively. Also shown in the figures for the upper data points are the inherent error bounds, obtained from Eqs. (12), on the calculated values of $C_V(\alpha, \beta)$ and α.

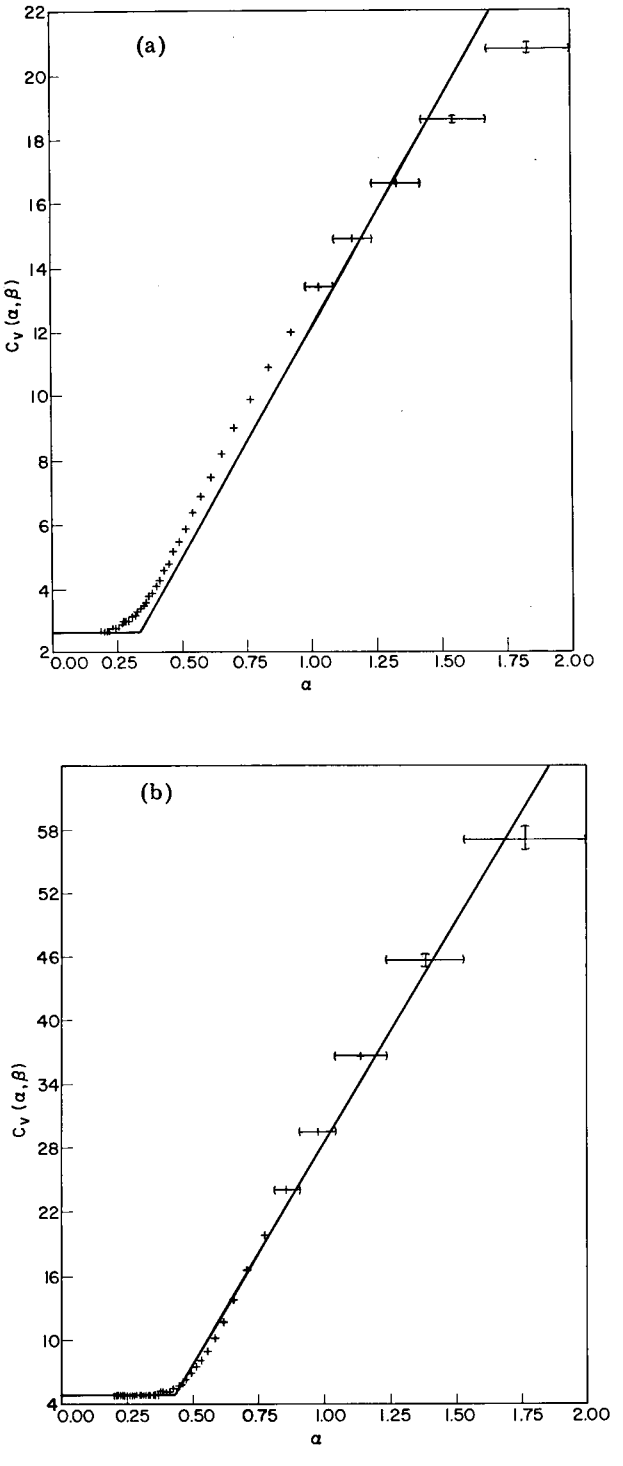

Fig. 5 — The calculated viscous damping coefficient $C_V(\alpha, \beta)$ vs the dimensionless amplitude α for (a) data set 1 (β = 430) and (b) data set 16 (β = 1520). The calculated points are indicated by the + symbol, and the inherent bounds on these points are enclosed by parentheses. The solid curve is the two-segment straight-line fit to the calculated points.

Each of these curves indicates that $C_V(\alpha, \beta)$ remains nearly constant (with a value depending on β) for a large range of low α and becomes linear with α as α becomes larger. Separating these two kinds of behavior is a short transition region. For small α, the constant behavior of C_V is in accord with theoretical predictions [6] and related experimental studies [1, 2]. Meanwhile, for larger α, the linear behavior of C_V with α agrees with the concept of velocity-squared damping. To show the latter point, suppose we had originally written the fluid force per unit length F_f as

$$F_f(\ddot{x}, \dot{x}) = -\frac{\pi}{4}\rho d^2 C_M(\alpha, \beta)\ddot{x} - 1/2\rho d C_D(\alpha, \beta)\dot{x}\,|\dot{x}| \tag{19a}$$

instead of, as in Eqs. (1) and (14),

$$F_f(\ddot{x}, \dot{x}) = -\frac{\pi}{4}\rho d^2 C_M(\alpha, \beta)\ddot{x} - \pi\rho\nu\beta^{1/2} C_V(\alpha, \beta)\dot{x}\,. \tag{19b}$$

Then the relationship between C_D and C_V, based on equivalent energy dissipation per cycle, is

$$C_D(\alpha, \beta) = (3\pi^2\beta^{-1/2}/16)\,[C_V(\alpha, \beta)/\alpha]\,. \tag{20}$$

Hence, for C_V proportional to α, $C_D(\alpha, \beta)$ becomes a constant dependent on β.

To develop useful engineering formulas for the viscous damping coefficient, the curve of $C_V(\alpha, \beta)$ vs α for each data set is approximated by a two-segment straight-line fit

$$C_V(\alpha, \beta) = C_1(\beta) + \left\{\frac{16}{3\pi^2}\,\beta^{1/2} C_2(\beta)[\alpha - \alpha_T(\beta)]\right\} U[\alpha - \alpha_T(\beta)]\,. \tag{21}$$

Here, U is the Heaviside unit step function defined by

$$U(\alpha - \alpha_T) = \begin{cases} 0 & \alpha < \alpha_T, \\ 1 & \alpha \geqslant \alpha_T, \end{cases} \tag{22}$$

and C_1, C_2, and α_T are the fitting coefficients. These coefficients are determined as follows:

a. Since $C_1(\beta)$ represents the nearly constant part of the curve of C_V vs α, it is directly related to that part of the amplitude decay curve given by $\ell n x_i \approx B_1 - B_3 i$ (see Eq. (15a)). Hence, from Eqs. (9b) and (14b), $C_1(\beta)$ is calculated as

$$C_1(\beta) = [(2k\tau/\pi^2)B_3 - c]/(\pi\rho\nu\beta^{1/2}), \tag{23}$$

with τ and β defined, respectively, by Eqs. (10b) and (13b) and with the required numerical values for each data set given in Tables 1 and 2.

b. The transition value of α, $\alpha_T(\beta)$, is defined as that value of α at which the nonlinear damping effects begin to have significance. We take, as an indication of this value, the location

of the minimum value of $C_V(\alpha, \beta)/\alpha$ as determined by a parabolic interpolation through the minimum calculated value of $C_V(\alpha, \beta)/\alpha$ and its left and right neighboring values.

c. The nonlinear damping coefficient $C_2(\beta)$ is obtained from a least-squares straight-line fit to the calculated values of $C_V(\alpha, \beta)$ and α for which $\alpha \geqslant \alpha_T$. Actually, this is an interesting case, as is seen from Figs. 5, in which the dependent variable $C_V(\alpha, \beta)$ has far less error associated with it than the independent variable α. For such a case, the appropriate least-squares value of $C_2(\beta)$ from Eq. (21) is (see Deming [5])

$$C_2(\beta) = \frac{3\pi^2}{16\beta^{1/2}} \frac{\sum_{\alpha \geqslant \alpha_T} w_\alpha [C_V(\alpha, \beta) - C_1(\beta)]^2}{\sum_{\alpha \geqslant \alpha_T} w_\alpha [C_V(\alpha, \beta) - C_1(\beta)] [\alpha - \alpha_T(\beta)]} \tag{24a}$$

Here, w_α is the weight associated with the calculated value of α. Since the relative error in α is $E_{\bar{x}}$, from Eq. (12c), we choose to weight α by its relative goodness. Thus, w_α is taken as

$$w_\alpha = 1 - E_{\bar{x}}. \tag{24b}$$

In Figs. 5a and 5b, the two-segment straight-line fit to the $C_V(\alpha, \beta)$-vs-α curve, obtained by the above procedure, is shown by the solid line.

A summary of the added mass and viscous damping coefficients is given in Table 3, which is ordered by increasing vibratory Reynolds number β. In addition to the associated value of β listed for each data set, cross-referenced to Table 1, are the added mass coefficient $C_M(\beta)$ and the curve-fitting parameters $C_1(\beta)$, $C_2(\beta)$, and $\alpha_T(\beta)$ for the viscous damping coefficient $C_V(\alpha, \beta)$.

From this table, one can see that, while certain trends with respect to β exist for the coefficients C_M, C_1, C_2, and α_T, the total variation in these coefficients over the range $230 < \beta < 5220$ is very small. Thus, these coefficients can be considered essentially constant over the range of β obtained in the experimental program. Hence, as a final step in developing empirical formulas for the added mass and viscous damping, the average values of these coefficients are used, and we take C_M, C_1, C_2, and α_T respectively as

$$C_M(\beta) = 1.01 \tag{25a}$$

$$C_1(\beta) = 4.50 \tag{25b}$$

$$C_2(\beta) = 1.68 \tag{25c}$$

$$\alpha_T(\beta) = 0.40. \tag{25d}$$

Table 3 — Summary of Added Mass and Viscous Damping Coefficients†

Data Set	$C_V(\alpha, \beta) = C_1(\beta) + \left\{\frac{16}{3\pi^2}\beta^{1/2}C_2(\beta)[\alpha - \alpha_T(\beta)]\right\} U[\alpha - \alpha_T(\beta)]$ (Eq. (21))				
	$\beta \times 10^{-3}$	$C_M(\beta)$	$C_1(\beta)$	$C_2(\beta)$	$\alpha_T(\beta)$
2	0.23	1.10	3.12	1.83	0.37
3	0.25	1.15	3.44	1.98	0.37
4	0.26	1.50	3.61	2.00	0.38
5	0.29	1.12	3.17	2.00	0.35
1	0.43	1.17	2.65	1.27	0.34
6	0.62	1.02	3.65	1.66	0.40
10	0.84	1.02	3.78	1.64	0.38
11	0.88	1.02	3.56	1.72	0.40
7	0.92	1.01	4.03	1.65	0.34
12	0.95	0.86	3.70	1.52	0.38
13	1.01	0.93	5.15	1.59	0.44
14	1.09	1.14	4.61	2.37	0.32
15	1.20	0.96	4.16	1.77	0.36
8	1.48	1.02	4.74	1.57	0.37
16	1.52	0.89	4.88	1.97	0.43
9	1.67	1.50	4.23	1.44	0.37
18	1.72	0.94	3.59	1.31	0.39
19	1.82	0.99	4.01	1.24	0.46
20	1.93	0.87	3.51	1.43	0.43
21	2.06	0.98	5.32	1.49	0.43
22	2.23	0.90	4.23	1.64	0.39
23	2.45	0.97	4.30	1.52	0.43
17	2.49	1.03	7.75	1.54	0.40
25	3.70	1.00	7.40	2.02	0.45
26	3.90	0.86	7.10	1.73	0.50
24	3.91	0.87	6.21	1.48	0.48
27	4.12	0.85	5.66	1.80	0.45
28	4.39	0.91	3.92	1.82	0.41
29	4.75	0.88	4.58	1.79	0.45
30	5.22	0.80	4.92	1.54	0.44

†Based on the values $\rho = 1.00$ g/cm^3 and $\nu = 0.01$ cm^2/s

DISCUSSION AND IMPLICATIONS

If we combine Eqs. (19b), (21), and (25), the empirical formula obtained in this report for the fluid force per unit length on a harmonically oscillating circular cylinder in the parameter range $\alpha < 2.00$ and $230 < \beta < 5220$ becomes

$$F_{fe}(\ddot{x}, \dot{x}) = -\frac{\pi}{4}\rho d^2(1.01)\ddot{x}$$

$$-\pi\rho\nu\beta^{1/2}\left\{4.50 + \left[\frac{16}{3\pi^2}\beta^{1/2}(1.68)(\alpha - 0.40)\right] U(\alpha - 0.40)\right\}\dot{x}. \qquad (26)$$

Here, the subscript e means "empirical." This formula should be compared to the commonly used expression of Eq. (19a) with $C_M = 1.00$ and $C_D = 1.20$, or

$$F_{fs}(\ddot{x}, \dot{x}) = -\frac{\pi}{4}\rho d^2(1.00)\ddot{x} - 1/2\rho d(1.20)\dot{x}|\dot{x}|, \qquad (27)$$

where the subscript s means "standard."

We see immediately from this comparison that little difference exists between the empirically obtained and commonly used fluid inertial loadings. However, this is not true for the fluid dampings. *These experiments show that the commonly used expression for the fluid damping is incorrect.* This has important implications for the design of offshore structures.

To understand some of these implications, it is useful to compare the energy dissipated per cycle as determined experimentally, D_e, to the energy dissipated per cycle as determined by the commonly used expression for the fluid damping, D_s. For the region of dimensionless vibration amplitudes where the empirically determined damping is purely viscous, the applicable dissipation ratio is found as

$$D_e/D_s = \frac{3\pi^2(4.50)}{16(1.20)}\frac{1}{\alpha\beta^{1/2}} = 6.94/\alpha\beta^{1/2}, \quad \alpha \leqslant 0.40. \qquad (28)$$

Equation (28) implies that, for $D_e/D_s < 1$, the commonly used value for damping is larger than the experimentally obtained value. This in turn implies, in a simple-minded sense and neglecting all other conditions, that the structure is underdesigned (too much damping has been assumed). Conversely, for $D_e/D_s > 1$, the commonly used damping value is smaller than the true value, and the structure is overdesigned (too little damping has been assumed). In either case, using the incorrect expression is costly, since an underdesigned structure is subject to failure and an overdesigned one is needlessly expensive.

In Fig. 6, contours of constant overdesign and underdesign (that is, contours of constant D_e/D_s) in the α - β plane are shown for the ranges of α and β in which Eq. (28) is valid.

SUMMARY

A series of experiments has been performed to determine the fluid loadings on an oscillating circular cylinder. The experiments encompassed ranges of dimensionless amplitude and vibrational Reynolds number given respectively by $\alpha < 2.00$ and $230 < \beta < 5220$. An empirical formula for the fluid loadings, valid within this range, is given by Eq. (26).

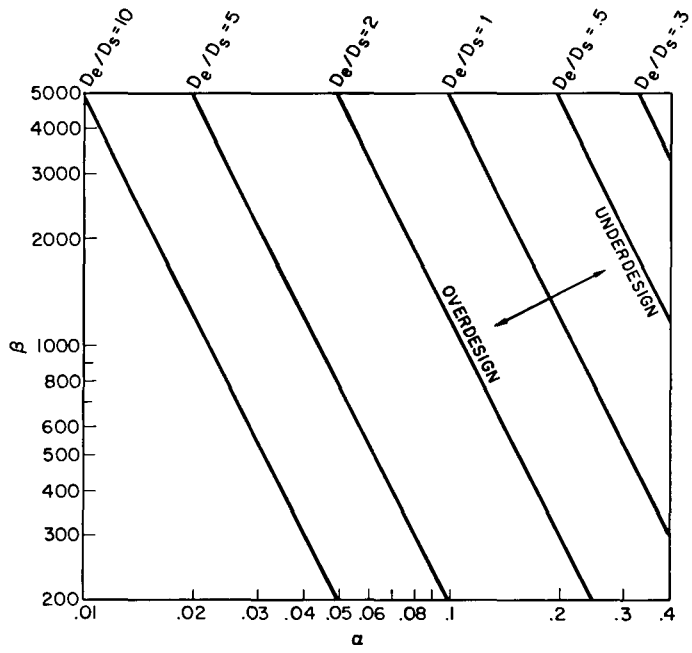

Fig. 6 — Contours of constant overdesign or underdesign, given by the ratio of energy dissipated per cycle as found experimentally, D_e, to the energy dissipated per cycle as calculated by the commonly used velocity-squared damping law, D_s.

This equation shows that the inertial component of the fluid loading found in the experiments is in agreement with the commonly used potential flow formula for the fluid inertial loading. However, the fluid damping as experimentally ascertained differs significantly from the commonly used velocity-squared damping. In particular, the experimental results revealed that

a. For $\alpha < 0.40$, the fluid damping is essentially viscous (linear),

b. For $\alpha > 0.40$, the fluid damping contains both linear and velocity-squared components.

The implications of using velocity-squared damping rather than the empirically derived damping formula of Eq. (26) in the design of ocean structures were also examined. Depending on the values of α and β, velocity-squared damping could produce an overdesigned or underdesigned structure as compared to a structure produced by using experimentally determined damping values.

In conclusion, we recommend that the damping formula of Eq. (26) be used henceforth for the design and analysis of circular cylindrical sections of ocean structures subjected to dynamic excitations. We also recommend that additional experiments be conducted to enlarge the parameter range encompassed by Eq. (26). Finally, because of the significant differences found here between the experimentally determined damping values and the commonly

used velocity-squared damping values, we suggest that added mass and damping measurements be undertaken for other cylindrical cross sections frequently used in ocean structures.

REFERENCES

1. J.T. Stuart and L. Woodgate, "Experimental Determination of the Aerodynamic Damping on a Vibrating Circular Cylinder," *Phil. Mag.* 46, 40-46 (1955).

2. S.E. Ramberg and O.M. Griffin, "Some Transverse Resonant Vibration Characteristics of Wire Rope with Application to Flow-Induced Cable Vibrations," NRL Report 7821, Dec. 1974.

3. *Handbook of Ocean and Underwater Engineering*, J.J. Myers, C.H. Holm, and R.F. McAllister, editors, McGraw-Hill, New York, 1969, Chap. 12, p. 45.

4. N. Minorsky, *Nonlinear Oscillations*, Van Nostrand, Princeton, N. J., 1962.

5. W.E. Deming, *Statistical Adjustment of Data*, John Wiley and Sons, New York, 1943.

6. G.G. Stokes, "On the Effect of the Internal Friction of Fluids on the Motion of Pendulums," *Trans. Cambridge Phil. Soc.* 9 (II), 8-106 (1851).